Atmospheric and Oceanic Science Letters xxx (xxxx) xxx

KeAi CHINESE ROOTS GLOBAL IMPACT

Contents lists available at ScienceDirect

Atmospheric and Oceanic Science Letters

journal homepage: http://www.keaipublishing.com/en/journals/atmospheric-and-oceanic-science-letters/

Long-term variations of the solar energy in different subregions of Northwest China and associated mechanisms

Junhui Yu [a], Hui Ma [b], Shen-Ming Fu [c,*], Xiaoling Su [a,*], Xiqiang Chang [c], Yanan Fu [b]

[a] School of Energy and Electrical Engineering, Qinghai University, Xining, China
[b] International Center for Climate and Environment Sciences, Institute of Atmospheric Physics, Chinese Academy of Sciences, Beijing, China
[c] State Grid Xinjiang Electric Power Co., Ltd., Urumqi, China

ARTICLE INFO

Keywords:
Solar energy
Surface solar radiation
Surface temperature
Northwest China

关键词:
太阳能
地表太阳辐射
地表气温
中国西北

ABSTRACT

As a type of clean and pollution-free energy source, solar energy plays an important role in achieving the goals of carbon neutrality and global sustainable development. Northwest China occupies an important position in the national energy strategy due to its rich solar energy. Clarifying the long-term variations of Northwest China's solar energy and understanding the associated mechanisms are crucial to improving the layout of new energy sources and the usage efficiency of solar energy within China. In this study, the authors first divide Northwest China into northwestern and southeastern sections by conducting a rotated empirical orthogonal function analysis on the surface solar radiation (SSR) from 1993 to 2022, and then explore the SSR's variation trends and associated mechanisms within these subregions. It is found that the two subregions, both of which show a significant feature of decadal change, differ notably in their long-term trends: the northwestern section shows a significant increasing trend of ~8.1 kJ m^{-2} yr^{-1} in the annual mean SSR, and in each season the SSR increases significantly, with a maximum/minimum increasing rate of ~11.2/~4.6 kJ m^{-2} yr^{-1} appearing in summer/autumn. A possible mechanism for the SSR's increasing trend is that global warming results in a lower relative humidity within the northwestern section, which decreases the total cloud cover, as it is harder for the atmosphere to reach saturation state. A decreasing total cloud cover results in an increasing SSR within the northwestern section. In contrast, the southeastern section shows no significant trend in annual mean SSR, as the SSRs in summer and autumn show significant decreasing trends, whereas the trends in spring and winter are not significant.

摘要

作为一种清洁无污染的新能源, 太阳能对于实现碳中和及可持续发展的目标至关重要. 西北地区太阳能资源丰富, 在我国能源战略中占据着重要地位. 厘清西北地区太阳能的长期变化趋势并揭示其可能的内在机理有助于改善我国的新能源布局并提高太阳能的利用效率. 鉴于此, 作者首先对1993年至2022年的地表太阳辐射 (SSR) 进行了旋转经验正交函数分析, 将西北地区划分为西北和东南两个分区, 然后分别研究了这些分区内SSR的变化趋势和相关机制. 研究发现, 在西北地区的两个分区内, SSR均表现出显著的年代际变化特征, 但两个分区内的SSR趋势存在显著不同. 对于西北分区而言, 其年平均SSR呈现出显著的增长趋势 (增速约为8.1 kJ m^{-2} yr^{-1}), 在每个季节, 其季节平均的SSR都显著增加, 最大与最小增速分别为11.2 (夏季) 和4.6 kJ m^{-2} yr^{-1} (秋季). 该区域内SSR增加趋势的一个可能机制是, 全球变暖导致该区域内相对湿度较低, 所以大气更难达到饱和状态, 这直接导致该区域内的总云量减少; 总云量的减少使得云对太阳短波辐射的反射, 散射和吸收减弱, 因此, 该区域内SSR增加. 对于东南分区而言, 由于其夏季和秋季的SSR呈显著的下降趋势, 而春季和冬季的SSR趋势并不显著, 所以该区域内年平均的SSR没有显著的线性趋势.

1. Introduction

Surface solar radiation (SSR) is the shortwave radiation received by the Earth's surface, which is emitted by the sun in the form of electromagnetic waves (Holton, 2004; Wild et al., 2005). SSR plays an important role in the Earth's energy balance, and acts as the main driving force for the Earth's weather systems (Fu et al., 2019; Wohland et al., 2020). Through the photoelectric effect, solar energy is converted into electrical energy (Besharat et al., 2013; Shang et al., 2023), which can be directly used in human society. This is of particular importance for achieving the goal of carbon neutrality and pursuing sustainable development (Gilgen et al., 1998; Wu et al., 2010; Wild, 2012; Wang et al., 2020), as solar energy is a type of clean and pollution-free energy, which has a huge reserve on Earth (Wild et al., 2005; Yao et al., 2023).

* Corresponding authors.
E-mail addresses: fusm@mail.iap.ac.cn (S.-M. Fu), suxiaoling@qhu.edu.cn (X. Su).

https://doi.org/10.1016/j.aosl.2024.100515
Received 7 March 2024; Revised 16 April 2024; Accepted 10 May 2024
Available online xxx

Please cite this article as: J. Yu, H. Ma, S.-M. Fu et al., Long-term variations of the solar energy in different subregions of Northwest China and associated mechanisms, Atmospheric and Oceanic Science Letters, https://doi.org/10.1016/j.aosl.2024.100515

As atmospheric states (e.g., aerosol, moisture, cloud, etc.) can affect SSR notably (Wang et al., 2020), for different regions, their SSRs show different responses to a warming climate (Wild et al., 2005; Dong et al., 2023). In order to improve the layout of new energy resources and to lift the usage efficiency of solar energy, a series of studies have been conducted for exploring the long-term trends of SSR within different regions, and understanding the mechanisms that govern the variations. For instance, based on long-term station observations from different countries, Wild et al. (2005) found that the SSR over Europe and North America mainly decreased throughout the 1950s–1970s, and then during the 1990s the trend reversed. Wohland et al. (2020) also found this reversal in the long-term trend of SSR within Europe by using the CERA20C reanalysis. Through comparisons among different reanalysis datasets, they proposed that the variations of aerosols were crucial for the change in the long-term trend. Zheng et al. (2012) analyzed the SSR in Beijing–Tianjin–Hebei and found an increasing trend in its eastern section. A decrease in cloud cover and a reduction in precipitation were the main reason for the increase in SSR. By using the daily solar radiation observed by 489 stations in China, Tao et al. (2016) detected significant decreasing trends in North China, Northeast China, and Southwest China from 1981 to 2014. Based on ERA5 and NCEP2 reanalysis data, Dong et al. (2023) determined increasing trends in the SSR within North America and Europe. These trends had strong seasonality, with the maximum increasing rate appearing in summer. Through different sensitivity simulations, they attributed the recent decadal trends of SSR in Europe to the reduction of anthropogenic aerosol emissions, whereas for North America they found the effects from sea surface temperature and sea-ice extent were more important.

Northwest China (Fig. 1(b)) plays an indispensable role in realizing China's carbon neutrality goal, as it is one of the regions with the most abundant solar energy all over the world (Wild et al., 2005; Wild, 2012; Cao and Zhu, 2021; Yao et al., 2023). Therefore, it is of particular importance to explore the long-term trend of SSR in Northwest China and to understand the underlying mechanisms. There are some studies on the long-term variation of SSR in Northwest China; however, they mainly took the region as a whole. Because the topography, land use, and precipitation show notably different features for different subregions of Northwest China (Li et al., 2008; Fu et al., 2020; Luo et al., 2020; Ma et al., 2023), it is necessary to explore the respective features of the SSR within different subregions. To this end, the primary purpose of this study is (i) to objectively divide Northwest China into different subregions based on the long-term spatiotemporal features of SSR; (ii) to clarify the respective long-term trends of SSR within different subregions; and (iii) to explore the possible mechanisms governing the long-term variations of SSR. The remaining parts of this paper are structured as follows: the data and methods are introduced in section 2; the results are presented in section 3; and a conclusion and some further discussion are given in section 4.

2. Data and methods

2.1. Data

The data used in this paper are the monthly mean field of SSR from 1993 to 2022 with a spatial resolution of 0.25° × 0.25° derived from the ERA5 reanalysis dataset (Hersbach et al., 2020). According to quantitative evaluation, these reanalysis data show an overall credible performance in representing the real SSR (He et al., 2016; Dong et al., 2023). In addition to SSR, the 2-m temperature (TMP), dewpoint temperature (Td), entire layer of precipitable water (PW), total cloud cover (TCC), convective available potential energy (CAPE), and altitude from the ERA5 dataset are used to understand the spatiotemporal features of the SSR in Northwest China. In order to avoid the SSR's trend reversal around 1990 (Wild et al., 2005), we use the period from 1993 to 2022 for analyses. This is consistent with the suggestion from the World Meteorological Organization, as 30 years of weather data is valid for creating a "normal" climate state for a location or region.

2.2. Methods

The methods used in this study mainly include empirical orthogonal function (EOF) analysis (Huang, 1999), rotated EOF analysis (REOF), linear trend analysis, and the Pearson correlation coefficient (CC). In statistical studies, EOF analysis has been widely used to decompose a four-dimensional meteorological field into a spatial and a temporal function component that are orthogonal to each other. In this study, we use the monthly mean SSR from 1993 to 2022 within 10°–60°N and 75°–135°E for the EOF analysis. REOF analysis is based on EOF by performing maximum-variance rotations on each load vector field (Horel, 1981). As the spatial distribution features obtained by REOF are clearer than those obtained by EOF, REOF is widely used for determining subregions (Li et al., 2016; Fu et al., 2016). In this study, we rotate the first three principal components of the EOF analysis, which have an accumulative variance contribution of ~88.5%. Based on the loading vector that possesses the largest variance contribution, we divide Northwest China into different subregions. The Pearson CC is used to evaluate the correlation between two variables, and least-squares regression is used to fit a linear model to a time series, with the slope indicating the linear trend (Huang, 1999). There is no *a priori* hypothesis based on some probability distribution and, hence, no statistical test for the EOF/REOF analyses (Huang, 1999). Student's *t*-test and the Mann–Kendall trend test (Mann, 1945) are used to verify the significance of the CC and the trend, respectively. The 95% confidence level ($p < 0.05$) is used to reflect whether the correlation/trend is significant.

3. Results

3.1. Regional divisions

We use the monthly mean SSR within China during a 30-yr period (from 1993 to 2022) for the EOF analysis (Horel, 1981). The accumulative variance contribution of the first three principal components is ~88.5% (not shown). After rotating the first principal component of EOF, we obtain the first loading vector of the REOF, which has a variance contribution of ~39.1% (Fig. 1(a)). As the first loading vector has a variance contribution much larger than those of the remaining two loading vectors, it is used to divide Northwest China. As Fig. 1(a) shows, most of China has a negative value of the loading vector, whereas the region at the upper-left corner of the graph has a positive value. The time coefficient of the first leading mode is illustrated in Fig. 1(b). It is shown that the time coefficient shows a significant feature of decadal change: the time coefficient is positive before 1994, and then during the period from 1994 to 2009 it changes to negative. This means that the spatial pattern shown in Fig. 1(a) reverses in this period. After that, from 2009 to 2022, the time coefficient becomes positive again (Fig. 1(b)), implying the spatial pattern restores. In summary, according to the first leading mode of the REOF analysis, we divide Northwest China into Region I (northwestern section of Xinjiang; Fig. 1(c)) and Region II (including the southeastern section of Xinjiang, Qinghai, Gansu, Shaanxi, and Ningxia). As Fig. 1(d) shows, the topographies within both subregions differ from each other significantly, which notably affect the horizontal distributions and temporal variations of SSR.

3.2. Horizontal distribution and long-term trend

As Fig. 2(a) shows, the annual mean SSR mainly decreases from south to north. The strongest SSR mainly appears over the Tibetan Plateau, where the altitude is above 3000 m (Fu et al., 2019, 2021), whereas the weakest SSR mainly appears in the northern section of Region I, where the altitude is mainly below 1000 m (Fig. 1(d)). The CC between the altitude and SSR is ~0.79 ($p < 0.05$), implying that the horizontal

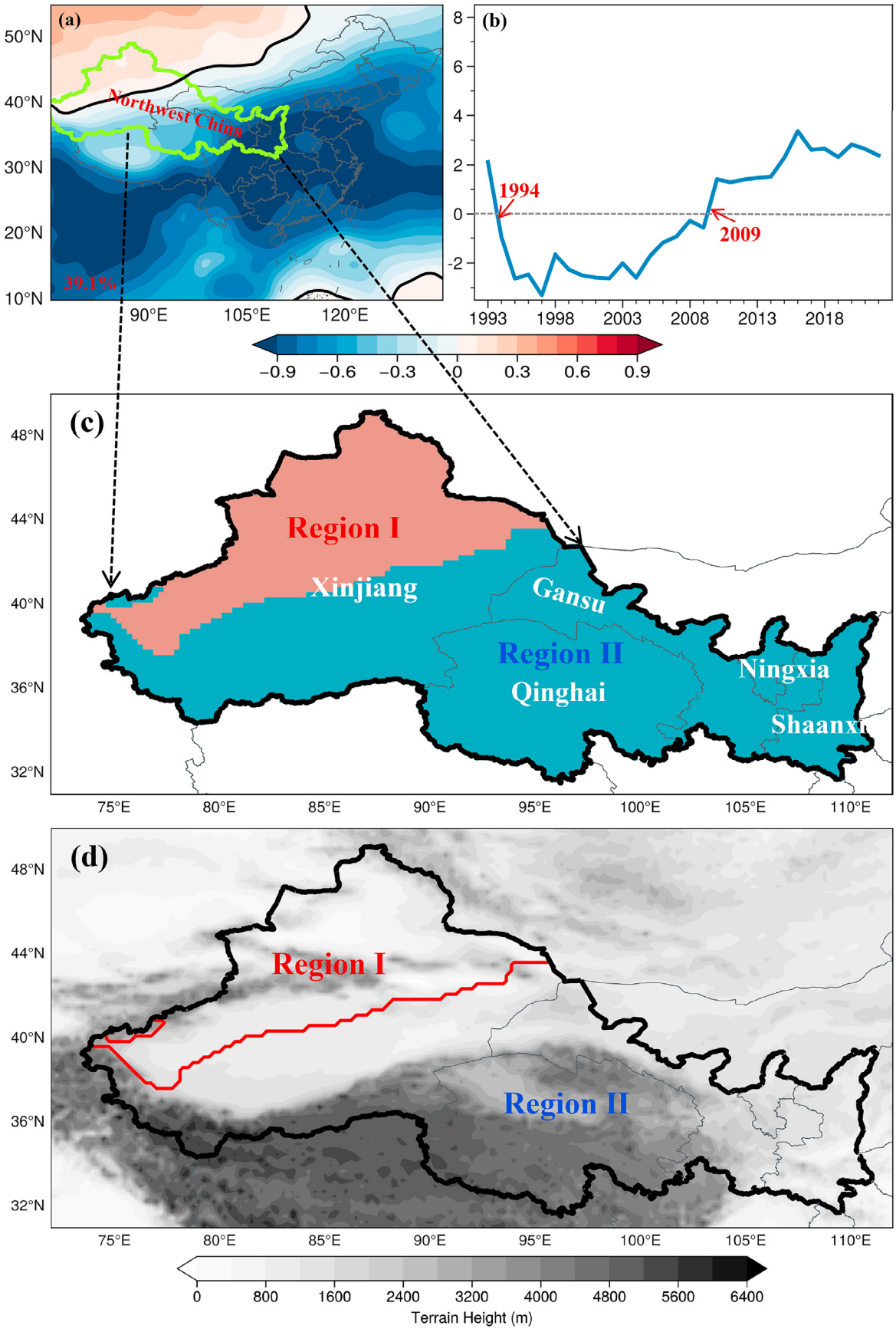

Fig. 1. (a) Spatial pattern of the first leading mode of the REOF (shading is the value of the loading vector, and the thick black contour is the zero contour). (b) Normalized time coefficient of the first leading mode. (c) Division of Region I (red shading) and Region II (blue shading) according to the REOF analysis results. (d) Topography (shading; units: m) of Region I and Region II.

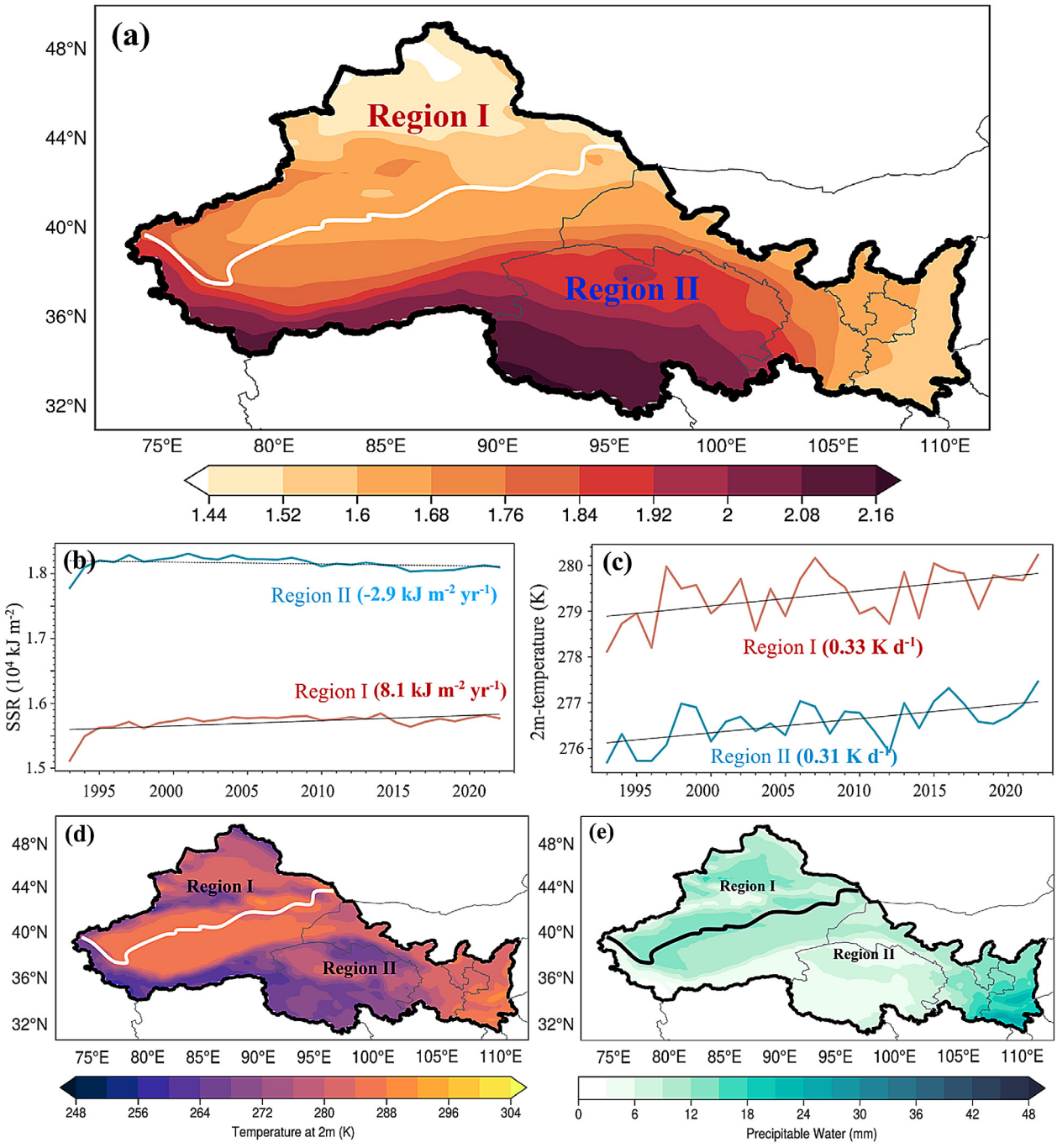

Fig. 2. (a) Annual mean SSR (shading; units: 10^7 J m^{-2}) during the 30-yr study period within Region I and Region II, where the thick white line is the boundary of the two subregions. (b) Annual variations of the spatially averaged SSR (units: 10^4 kJ m^{-2}) within Region I and Region II, in which the solid black line represents the trend exceeding the 95% confidence level and the black dashed line represents the trend exceeding the 90% confidence level. (c) Annual variations of the spatially averaged 2-m temperature (units: K) within Region I and Region II, in which the black solid line represents the trend exceeding the 95% confidence level. (d) Annual mean 2-m temperature (shading; units: K) during the 30-yr study period within Region I and Region II, where the thick white line is the boundary of the two subregions. (e) Annual mean precipitable water (shading; units: mm) during the 30-yr period within Region I and Region II, where the thick black line is the boundary of the two subregions.

distribution of SSR is highly consistent with the distribution of the topography. The annual mean TMP and PW (Fig. 2(d, e)) are also highly correlated with the topography (Fig. 1(d)), as the CCs between them and altitude are around −0.91 ($p < 0.05$) and −0.85 ($p < 0.05$), respectively. As mentioned above, topography is a key feature for determining the climatological features of Northwest China. In addition, the CC between SSR and TMP is around −0.55 ($p < 0.05$), and the CC between SSR and PW is around −0.58 ($p < 0.05$), implying that there is a close relationship between SSR and TMP/PW (through affecting rainfall and cloud).

In terms of annual variations, Region I differs from Region II significantly (Fig. 2(b, e)). For the former, its area-averaged SSR is weaker in intensity than that of the latter, whereas its area-averaged TMP is higher. The two subregions show a similar increasing rate (~0.3 K/10 yr) in their TMP, which is a sign for global warming. However, under a similar warming rate, Region I shows a significant increasing trend of

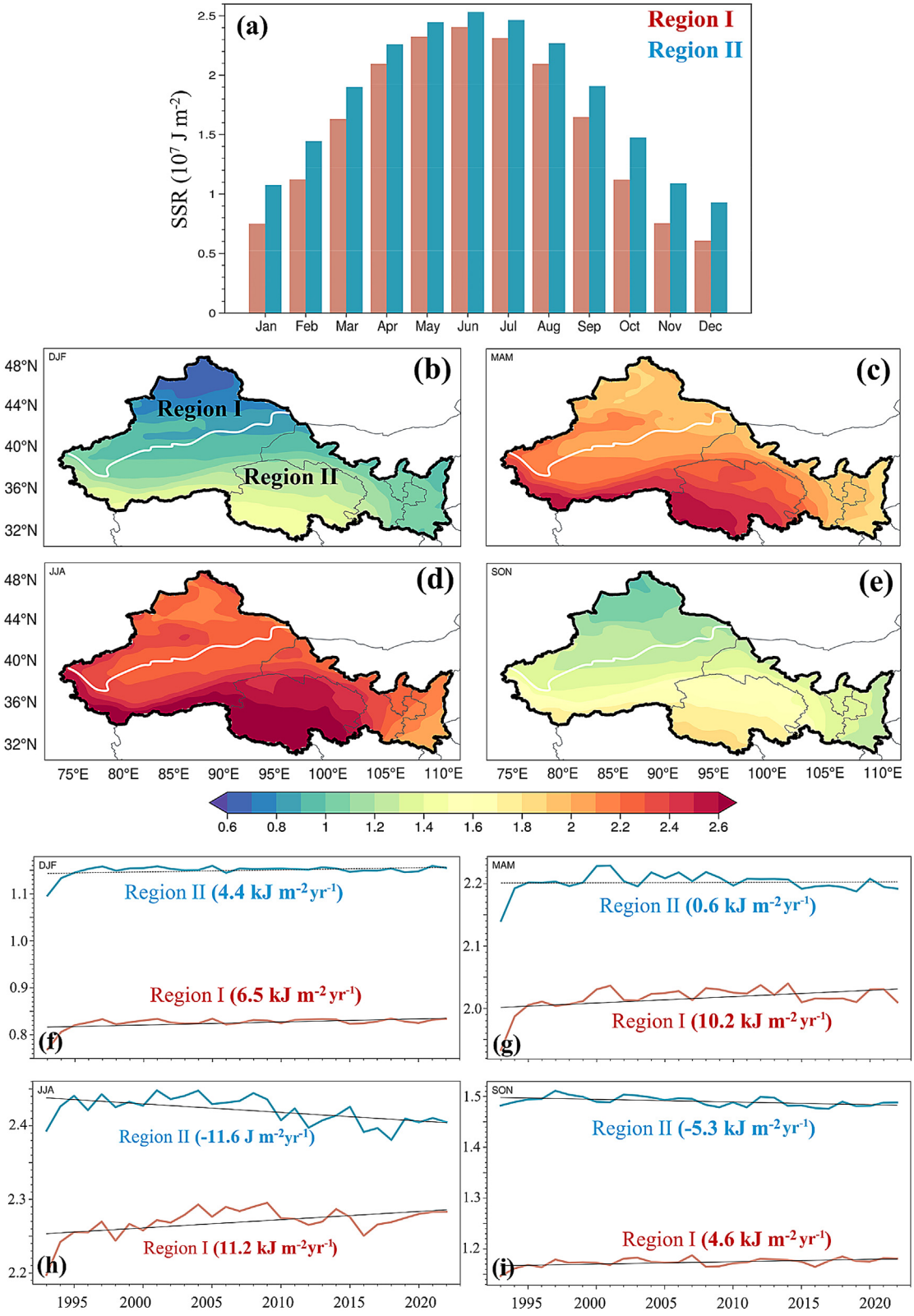

Fig. 3. (a) Monthly variation of the Region I/II averaged SSR (units: 10^7 J m^{-2}) during the 30-yr study period. (b–e) Temporally averaged SSR of different seasons (units: 10^7 J m^{-2}) during the 30-yr study period. DJF = December, January, and February (winter); MAM = March, April, and May (spring); JJA = June, July, and August (summer); and SON = September, October, and November (autumn). (f–i) Seasonal variations of the spatially averaged SSR (units: 10^7 J m^{-2}) within Region I and Region II, in which the black solid line represents the trend exceeding the 95% confidence level and the black dashed line represents the trend exceeding the 90% confidence level.

8.1 kJ m^{-2} yr^{-1}, which exceeds the 95% confidence level, whereas there is only a weak decreasing trend of −2.9 kJ m^{-2} yr^{-1} within Region II, which cannot pass the significance test. This means that the factors governing the long-term variations of SSR are different for Region I and Region II.

3.3. Seasonal variations

Overall, in each month and season, the area-averaged SSR is larger for Region II (Fig. 3(a, f–i)), which is similar to the contrast in the annual mean SSRs. The SSR in both Region I and Region II is characterized by a notable monthly variation (Fig. 3(a)): from January to June, the SSR in both subregions increases with time and reaches a maximum in June (the rate of increase is larger for Region I), and then from June to December it decreases with time (the rate of decrease is larger for Region I) and reaches a minimum in December. In terms of seasonal mean SSR, the minimum SSR appears in winter (Fig. 3(b)), the maximum SSR appears in summer (Fig. 3(d)), and the SSR in spring is stronger than that in autumn (Fig. 3(c, e)). As the seasonal variation of SSR is significant, it is necessary to analyze its long-term trend in each season.

As Fig. 3(f–i) shows, for Region I, in each season, its area-averaged SSR shows a significant increasing trend (exceeding the 95% confidence level), implying a better prospect for the usage of solar energy in this area. The fastest rate of increase appears in summer (~11.2 kJ m^{-2} yr^{-1}; Fig. 3(h)), whereas autumn has the slowest rate (~4.6 kJ m^{-2} yr^{-1}; Fig. 3(i)). In addition, the rate of increase in winter (~6.5 kJ m^{-2} yr^{-1}; Fig. 3(f)) is smaller than that in spring (~10.2 kJ m^{-2} yr^{-1}; Fig. 3(g)). Overall, the seasonal increasing trends are consistent with the increasing trend of ~8.1 kJ m^{-2} yr^{-1} in the annual mean SSR within Region I (Fig. 2(b)). For Region II, in winter and spring, the seasonal mean SSR only shows a weak increasing trend that cannot pass the significance test (Fig. 3(f, g)). In contrast, in summer and autumn, SSR shows a significant decreasing trend, exceeding the 95% confidence level (Fig. 3(h, i)), thereby implying a deteriorating prospect for the usage of solar energy in these seasons. Significant increasing trends are detected in the PW (i.e., the moisture condition for producing cloud becomes better) within Region II during summer and autumn (not shown). This is a possible reason for the decreasing trends of SSR as more cloud tends to result in more reflection, scattering, absorption, which reduce the SSR. The decreasing trend in summer (around −11.6 kJ m^{-2} yr^{-1}; Fig. 3(h)) is stronger than that in autumn (around −5.3 kJ m^{-2} yr^{-1}; Fig. 3(i)), which is similar to the intensity contrast in the rates of increase in Region I for these two seasons. The opposite long-term trends in different seasons may be a reason why the annual mean SSR within Region II shows no significant long-term trend.

3.4. Possible mechanisms

To explore the possible mechanisms for the long-term variations of the annual mean SSR within different subregions of Northwest China, we mainly focus on two factors (Wild et al., 2005; Zheng et al., 2012; Wohland et al., 2020; Dong et al., 2023): one is the cloud (affects SSR mainly through reflection, scattering, absorption, etc.), and the other is moisture (mainly through absorbing and forming cloud/rainfall). For Region I, as Table 1 shows, TCC shows a significant negative correlation with SSR (CC = −0.55), implying that TCC may be a governing factor for the long-term variation of SSR. A possible mechanism is that, as TMP shows a significant correlation with the difference between TMP and Td (DT; CC = 0.53), a warming climate would render a larger DT. A larger DT means the relative humidity is lower, and thus it becomes harder for the atmosphere to reach saturation state. In this situation, less cloud would be produced, which can be reflected by the significantly negative correlation between DT and TCC (CC = −0.73; Table 1). As TCC becomes smaller, its reflection, scattering and absorption of the solar shortwave radiation all weaken, and therefore SSR would become stronger (the CC between TCC and SSR is −0.55; Table 1). Unlike Region I, there is no significant correlation between TCC and SSR within Region II (CC = −0.28, which cannot pass the significance test). This indicates that, in addition to TCC, other factors such as aerosols, moisture and precipitation may also exert notable effects on SSR within Region II. In fact, compared to Region I, population density (anthropogenic aerosol), relative humidity (moisture content in the atmosphere) and rainfall are all larger for Region II (Tao, 1980; Li et al., 2008), which means their impacts on SSR would be stronger.

Table 1 Correlation coefficients between spatially averaged variables within Region I during the 30-yr study period, where bold font indicates exceedance of the 95% confidence level. SSR = surface solar radiation; TMP = 2-m temperature; PW = precipitable water; CAPE = convective available potential energy; DT = difference between TMP and dewpoint temperature; TCC = total cloud cover.

	TMP	PW	CAPE	DT	TCC
SSR	**0.49**	**−0.45**	**−0.41**	**0.63**	**−0.55**
TMP	/	0.21	−0.27	**0.53**	**−0.40**
PW	0.21	/	**0.69**	**−0.66**	**0.51**
TCC	**−0.40**	**0.51**	/	**−0.73**	/

4. Conclusion and discussion

As one of the regions with the most abundant solar energy all over the world, Northwest China plays an indispensable role in achieving the goal of carbon neutrality in China. Therefore, it is important to explore the long-term trend of SSR in Northwest China and to understand the underlying mechanisms, because the results are helpful for improving the layout of new energy resources and for lifting the usage efficiency of solar energy in China. After conducting an REOF analysis on the ERA5 SSR from 1993 to 2022, we find that Northwest China can be divided into Region I and Region II according to the first leading mode. Overall, Region I differs from Region II notably in terms of topography, which notably affects the horizontal distributions and temporal variations of SSR.

Overall, Region I and Region II show similar rates of increase in their surface temperature (~0.3 K/10 yr), which is consistent with global warming. However, under a warming climate, SSR shows different responses in the two subregions: significant increasing trends of SSR are detected in each season (the fastest rate of increase of ~11.2 kJ m^{-2} yr^{-1} appears in summer, and the slowest rate of ~4.6 kJ m^{-2} yr^{-1} appears in autumn), and all year (~8.1 kJ m^{-2} yr^{-1}) within Region I, implying a better prospect for the usage of solar energy in this area. In contrast, Region II does not show a significant trend in the annual mean SSR, because significant decreasing trends are found in summer and autumn, while in the other seasons the increasing trends are not significant. This means that the factors governing the long-term variations of SSR are different for Region I and Region II. A possible mechanism for the long-term increasing trend of the annual mean SSR within Region I is that a warming climate would cause an increase in the difference between temperature and dewpoint temperature (the CC between TMP and Td is 0.53; $p < 0.05$). A larger difference between temperature and dewpoint temperature means the relative humidity becomes lower, and thus it becomes harder for the atmosphere to reach saturation state. Further analysis indicates that, within Region I, the 2-m dewpoint temperature shows a significant decreasing trend of around −0.26 K/10 yr, which confirms this result. Consistent with a lowering relative humidity within Region I, less cloud is generated (the CC between DT and TCC is −0.73; $p < 0.05$), which can be confirmed by a significant decreasing trend in TCC (−0.01/10 yr/; $p < 0.05$). Therefore, the reflection, scattering and absorption of the solar shortwave radiation due to the cloud all weaken. In this situation, SSR would become stronger (the CC between TCC and SSR is −0.55; $p < 0.05$). It should be noted that the decreasing trend in TCC is in sharp contrast to the humidification in Northwest China (Zhang et al., 2021, 2023), which is represented by an increasing trend

in precipitation. One possible reason is that there are no significant linear correlations between TCC and precipitation, as many clouds do not produce rainfall, and under the same size conditions, the precipitation generated by cumulus clouds is much stronger than that of stratiform clouds (Mai et al., 2020). Different from Region I, there is no significant correlation between TCC and SSR within Region II, implying other factors such as aerosols, moisture and precipitation may also exert notable effects on SSR within Region II.

Funding

This research was supported by the National Key R&D Program of China [grant number 2022YFB2403002].

Acknowledgements

The authors sincerely thank the ECMWF for providing the ERA5 reanalysis data.

References

Besharat, F., Dehghan, A.A., Faghih, A.R., 2013. Empirical models for estimating global solar radiation: A review and case study. Renew. Sust. Energ. Rev. 21, 798–821.
Cao, M., Zhu, X.C., 2021. Spatial simulation and spatiotemporal changes analysis of total solar radiation on the earth's surface in China. J. Meteorol. Res. App. 42, 24–28.
Dong, B., Sutton, R.T., Wilcox, L.J., 2023. Decadal trends in surface solar radiation and cloud cover over the North Atlantic sector during the last four decades: Drivers and physical processes. Clim. Dyn. 60, 2533–2546.
Fu, S.M., Li, D.S., Sun, J.H., Si, D., Ling, J., Tian, F.Y., 2016. A 31-year trend of the hourly precipitation over South China and the associated mechanisms. Atmos. Sci. Lett. 17, 216–222.
Fu, S.M., Mai, Z., Sun, J.H., Li, W.L., Ding, D., Wang, Y.Q., 2019. Impacts of convective activity over the Tibetan Plateau on plateau vortex, southwest vortex, and downstream precipitation. J. Atmos. Sci. 76, 3803–3830.
Fu, S.M., Jin, S.L., Shen, W., Li, D.Y., Liu, B., Sun, J.H., 2020. A kinetic energy budget on the severe wind production that cause a serious state grid failure in Southern Xinjiang China. Atmos. Sci. Lett. 2020, e977.
Fu, S.M., Mai, Z., Sun, J.H., Li, W.L., Zhong, Q., Sun, J.R., Zhang, Y.C., 2021. A semi-idealized modeling study on the long-lived eastward propagating mesoscale convective system over the Tibetan Plateau. Sci. China Earth Sci. 64, 1996–2014.
Gilgen, H., Wild, M., Ohmura, A., 1998. Means and trends of shortwave irradiance at the surface estimated from Global Energy Balance Archive data. J. Clim. 11, 2042–2061.
He, X.F., Yuan, C.H., Yang, Z.B., 2016. Performance evaluation of Chinese solar radiation forecast based on three global forecast back ground fields. Acta Energiae Solaris Sin. 37, 897–904.
Hersbach, H., Bell, B., Berrisford, P., Hirahara, S., Horányi, A., Muñoz-Sabater, J., Nicolas, J., et al., 2020. The ERA5 global reanalysis. Q. J. R. Meteorol. Soc. 146, 1999–2049.
Holton, J.R., 2004. An introduction to dynamic meteorology. Academic Press, San Diego, p. 552.
Horel, J.D., 1981. A rotated principal component analysis of the interannual variability of the Northern Hemisphere 500 mb height field. Mon. Wea. Rev. 109, 2080–2092.
Huang, J.Y., 1999. Statistic analysis and forecast methods in meteorology. China Meteorological Press, Beijing, p. 385.
Li, D.S., Sun, J.H., Fu, S.M., Wei, J., Wang, S.G., Tian, F.Y., 2016. Spatiotemporal characteristics of hourly precipitation over central eastern China during the warm season of 1982–2012. Int. J. Climatol. 36, 3148–3160.
Li, W.L., Wang, K.L, Fu, S.M, Jiang, H., 2008. The interrelationship between regional westerly index and the water vapor budget in Northwest China. J. Glaciol. Geocryol. 30, 28–34.
Luo, Y.L., Sun, J.S., Li, Y., Xia, R.D., Du, Y., Yang, S., Zhang, Y.C., et al., 2020. Science and prediction of heavy rainfall over China: Research progress since the reform and opening-up of the People's Republic of China. J. Meteorol. Res. 78, 419–450.
Ma, H., Li, G.Q., Zeng, C.K., Wang, F., Jin, S.L., Fu, S.M., 2023. Evolutionary mechanisms of the strong winds associated with an intense cold wave event and their effects on the wind power production. Front. Earth Sci. 10, 1054037.
Mai, Z., Fu, S.M., Sun, J.H., Hu, L., Wang, X.M., 2020. Key statistical characteristics of the mesoscale convective systems generated over the Tibetan Plateau and their relationship to precipitation and southwest vortices. Int. J. Climatol. 36, 3148–3160.
Mann, H.B., 1945. Nonparametric tests against trend. Econometrica 13, 245–259.
Shang, Y.P., Guo, J.H., Song, Y., Liu, W.J., Ma, W.J., Li, W., 2023. Research on short-term irradiance prediction based on WRF-Solar model and SCA correction. Acta Energiae Solaris Sin. 44, 274–279.
Tao, S. Y., 1980. Rainstorms in China. Sci. Press, Beijing, p. 225.
Tao, S.L., Qi, Y.M., Shen, S.H., Li, Y.H., Zhou, Y., 2016. The spatial and temporal variation of solar radiation over China from 1981 to 2014. J. Arid Land Resourc. Environ. 30, 143–147.
Wang, J.M., Sun, X., Sun, R., Li, Z.M., Guo, R.L., He, M.L., 2020. Comparison of reanalysis radiation data and observations in China for 2000–2016. J. Trop. Meteorol. 36, 734–743.
Wild, M., Gilgen, H., Roesch, A., Ohmura, A., Long, C.A., Dutton, E.G., Forgan, B., et al., 2005. From dimming to brightening: Decadal changes in solar radiation at Earth's surface. Science 308, 847–850.
Wild, M., 2012. Enlightening global dimming and brightening. Bull. Am. Meteorol. Soc. 93, 27–37.
Wohland, J., Brayshaw, D.J., Bloomfield, H., Wild, M., 2020. European multidecadal solar variability badly captured in all centennial reanalyses except CERA20C. Environ. Res. Lett. 15, 104021.
Wu, Q.Z., Wang, Z.F., Cui, Y.J., 2010. Evaluating the solar radiation resources of China in recent 20 years by meteorological model. J. Appl. Meteorol. Sci. 21, 343–351.
Yao, D.G., Liu, W.J., Han, Y.X., Li, Z., Liang, Y., 2023. Construction and validation of the R models for short-term solar irradiance forecasting. Arid Land Geogr. 46, 47–55.
Zhang, Q., Zhu, B., Yang, J.H., Yu, H.P., Yue, P., Liu, X.Y., Lin, Q.Q., et al., 2021. New characteristics about the climate humidification trend in Northwest China. Chin. Sci. Bull. 66, 3757–3771.
Zhang, H.L., Han, F.Q., Zhang, L., Wang, L.X., Sun, Y., Li, F.M., 2023. Analysis of spatial and seasonal variations in climate warming and humidification in Northwest China. Arid Zone Res. 40, 517–531.
Zheng, Y.F., Yin, Z.Y., Wu, R.J., Liu, J.J., 2012. Analyses on variation and cause of surface solar radiation in Beijing, Tianjin and Hebei regions from 1960 to 2005. Plateau Meteorol. 31, 436–445.